

Title:

High Chromium Cast Irons: Destabilized-Subcritical Secondary Carbide Precipitation and Its Effect on Hardness and Wear Properties

Authors:

María Agustina Guitar, Sebastián Suárez, Orlando Prat, Martín Duarte Guigou, Valentina Gari, Gastón Pereira, Frank Mücklich

This is a post-peer-review, pre-copyedit version of an article published in *Journal of Materials Engineering and Performance*

The final authenticated version is available online at: <https://doi.org/10.1007/s11665-018-3347-1>

Cite as:

Guitar, M.A., Suárez, S., Prat, O. et al. J. of Materi Eng and Perform (2018) 27: 3877. <https://doi.org/10.1007/s11665-018-3347-1>



High chromium cast irons: destabilized-subcritical secondary carbide precipitation and its effect on hardness and wear properties.

María Agustina Guitar^{1,a}, Sebastián Suárez¹, Orlando Prat², Martín Duarte Guigou^{3,4},
Valentina Gari³, Gastón Pereira⁴, Frank Mücklich¹

¹ Department of Materials Science, Saarland University. Campus D3.3, D-66123,
Saarbrücken, Germany.

² Departamento de Ingeniería de Materiales, Universidad de Concepción, Edmundo
Larenas 270, Concepción, Chile

³ Programa de Ingeniería de Materiales, Facultad de Ingeniería y Tecnologías,
Universidad Católica del Uruguay, Av. 8 de Octubre 2738 - CP 11600, Montevideo,
Uruguay.

⁴ Laboratorio de Desarrollo de Nuevos Materiales, Tubacero S.A., Cnel. Raíz 949 -
CP12900, Montevideo, Uruguay.

Corresponding author: a.guitar@mx.uni-saarland.de - Tel./Fax: +49 681 302

70521/70502

ABSTRACT

This work evaluates the effect of a destabilization treatment combined with a sub-critical diffusion (SCD) and a subsequent quenching (Q) steps on precipitation of secondary carbides and their influence on the wear properties of HCCI (16%Cr). **The destabilization of the austenite at high temperature leads to a final microstructure composed by eutectic and secondary carbides, with an M_7C_3 nature, embedded in a martensitic matrix.** An improved wear resistance was observed in the SCD+Q samples in comparison to the Q one, which was attributed to the size of secondary carbides.

Keywords: High chromium white cast iron – Solid state transformation – secondary carbides precipitation – Wear - microstructure

Introduction

High Chromium Cast Irons (HCCI) have been a material of choice for wear resistant components in the mining and mineral processing industries for a long time, given their outstanding wear and erosion resistance [1]. The main reason for such resistance can be found in the hard M_nC_m reinforcement carbides embedded within the metallic matrix, being those of hypoeutectic, eutectic or hypereutectic origin [2,3]. Hypoeutectic compositions are the main group of materials in use in the industry, with compositions described in the ASTM standard A532 groups II and III [4]. Although hypereutectic HCCI would show a higher carbide volume fraction than hypoeutectic HCCI and it could be considered as a much more efficient wear resistant material; however, their low castability severely hinder their practical manufacture and use [5].

The microstructure and mechanical properties of HCCI are a direct consequence of the eutectic carbide content, matrix microstructure and the presence of secondary carbides embedded within the metallic matrix [6]. Particularly, the presence of secondary carbides has shown to improve the wear resistance behavior of the entire composite [2]. Secondary and also eutectic carbides characteristics are strongly influenced by the content of its main constituents (C, Cr) [2,3,7], minor alloying elements (Mo, Ti, V, Nb, W) [8–12] and thermal processing [5,13].

The wear resistance and mechanical properties, especially the hardness, of HCCI depend on the type, morphology and distribution of carbides, and on the nature of the supporting matrix structure which, in turn, depends on the chemical composition and on any subsequent thermal treatments [14–16]. The secondary carbides, may increase the wear resistance of the matrix itself, providing load support and reducing damage by third bodies scratching the surface, by the same mechanisms that has been studied carefully

with more conventional, low reinforcement volume fraction, composite materials [17,18]. To some extent, the precipitation of secondary carbides should lead to a more bimodal-like reinforced composite behavior, which has been proved previously to have a better wear performance than its mono modal counterparts [19,20].

Besides, the secondary carbides which precipitate in the matrix regions also influence wear resistance by increasing the matrix strength through dispersion strengthening and microstructure refinement, the fine secondary carbides can increase the mechanical support of the eutectic carbides. [10,11,21].

Precipitation of secondary carbides during a sub-critical destabilization treatment [22] has been previously described for HCCI and the usual quenching procedure, i.e. holding temperatures above the critical line (from 0.5 to 4 hours) before cooling in air. In most cases the authors compared the latter to a series of sub-critical approaches as references [11,23,24]. Heat treatments are designed to precipitate a fine dispersion of Fe-Cr carbides within the matrix. Multi-step treatments have been proposed (martensite formation and post-quench sub-critical annealing for carbide precipitation), with a significant secondary carbide precipitation, although the intermediate air cooling induced a sharp decrease in mechanical properties. The decrease in mechanical properties was associated with the formation of ferrite phases in the sub-critical step; in general sub-critical treatments have been associated with hardness reduction [25]. Furthermore, the type, size and distribution of secondary carbides formed during the destabilization depend on the composition and destabilization temperature. The secondary carbides are efficient for improving the abrasion resistance [26,27].

The proposed destabilized plus sub-critical diffusion treatment should lead to a sharper increase in size and a better distribution of secondary carbides within the matrix, without

affecting other mechanical properties. Assuming that this material behaves tribologically as a bimodal size reinforced MMC, the post treatment wear resistance should improve, despite the slight changes in other mechanical properties [23,28].

In this work, contrary to other works found in the literature [25], a destabilization process is carried out followed directly by a sub-critical diffusion (SCD) step in order to precipitate and grow secondary carbides. The main objectives of the present work are: (a) to analyze if increased secondary carbide precipitation is achievable with a high temperature destabilization and multi-step sub-critical heat treatment, using limited minor alloying elements and preserving mechanical properties; (b) to compare such results with a standard above critical destabilization treatment and (c) to analyze the effect of such increased carbide precipitation on wear resistance.

Experimental

HCCI samples were manufactured in arc furnace and casted in cubic sand molds. Chemical composition was determined by Emission Spectroscopy methods using a GNR Metal Lab 75/80 Optical Emission Spectroscope. The chemical composition of the studied HCCI is: C (2.43 wt.%) - Si (0.47 wt.%) – Mn (0.76 wt.%) – Cr (15.84 wt.%) - Ni (0.41 wt.%) – S (0.02 wt.%) – P (0.02 wt.%) – Cu (0.04 wt.%) – Fe (balance).

The thermal treatments were carried out by two methods: (i) destabilization above critical temperature (1253 K) and quenching and (ii) destabilization followed by a sub-critical diffusion (SCD) process at 923 K for 12 h. Destabilization temperature was determined as critical temperatures plus 50 K and SCD temperature was set at 50 K below zero-transformation-temperature for the corresponding chemical composition for maximum carbide precipitation. Thus, observations were carried out in four samples: (1) as cast conditions, (2) SCD, (3) Quenched (Q) and (4) SCD + Q; being the SCD sample an intermediate state. Schematic representation for each treatment is shown in Figure 1.

The samples were **ground** with embedded diamond discs (up to grit 1200) and polished using diamond powder suspensions up to 1 μm mean diameter. The samples were etched with Vilella's reagent (1 g picric acid + 5 ml HCl 100 ml ethanol) for 30 seconds at room temperature. Optical microscopy observations were carried out in all samples using a Leica CTR6000 microscope and images were acquired using a Jenoptik CCD Camera.

SEM characterization was carried out with a FE-SEM Helios Nanolab 600 (FEI company) working with an acceleration voltage of 10 kV and a 1.4 nA beam current. For a proper contrast between phases, a high sensitivity solid state backscattered electrons detector (vCD) was used. Electron Backscattered Diffraction with an acceleration voltage of 20

kV and 11 nA beam current together with the TSL OIM Data Collection software were used for the carbide type identification.

Macro-hardness on the Rockwell C scale was measured using a Wilson durometer with a diamond indenter and 150 Kgf load. Micro hardness was measured with a Leica Vickers microindenter applying 0.500 Kgf load on all samples for both, matrix and primary carbides. The indentation time in all cases was 15 s.

X-ray diffraction testing was performed with a PANalytical Empyrean X-ray diffractometer. The diffractograms were obtained using a symmetrical θ — θ geometry configuration and a Cu $K\alpha_1$ radiation ($\lambda = 0.15406$ nm). The incident and diffracted optical geometries were parallel and the diffraction angle (2θ) was varied from 25° to 100° with a step size of 0.013° and a 50 s/step rate. The applied voltage and current were 40 kV and 40 mA, respectively. For the phase identification and indexing, the High Score Plus software and ICDD Database were used.

Wear test was carried out in a CSM macro tribometer in rotational mode using an alumina pin, applying a 5N load for 4000 laps with 2.46mm radius at a speed of 5.0 cm/s with environment conditions set at 298 K (25 °C) and 45% humidity. Wear tracks were observed using a Zygo NewView 7300 white light interferometer (for wear volume calculations) and SEM microscopy.

Results and Discussion

Phase and microstructural evolution

Figure 2 shows the XRD measurements for the different states of the treated samples. The as-cast condition is represented by the eutectic carbide embedded in an austenitic matrix ($M_7C_3/Fe-\gamma$), as described in [25] and also predicted in the Jackson's diagram for the Fe-Cr-C system [29]. Some authors also reported the presence of martensite surrounding the eutectic carbide particles as a result of the excessive consumption of C and Cr by the eutectic carbides [25]. Consequently, the matrix remain depleted in these elements, resulting in the increase of the M_s temperature and promoting the martensite formation.

The SCD treatment lead to the transformation of the matrix from austenite to ferrite and carbides of the form M_7C_3 were detected. XRD measurements confirms the absence of martensite in this sample, whose presence is not expected since the sample was cooled in air after the sub-critical diffusion treatment. On other way, the quenching of the material (Q sample) generates a complete martensitic transformation of the matrix. Very small peaks corresponding to M_7C_3 are also observed. The SCD+Q sample showed, just like the Q sample, a matrix formed by martensite and carbides of the form M_7C_3 . In the inset of Figure 2, the most intense peaks from ferrite and martensite are shown. A shift in the diffraction angle and an increasing width of the peak, as a consequence of the lattice distortion, allow the identification of martensite form ferrite.

In order to corroborate the obtained phases in the Q and SCD+Q samples, thermodynamic calculations with the Thermo-Calc software and EBSD measurements were performed, see Figure 3. The simulation was performed using all the elements of the studied alloy (as shown in Table 1), and using the TCFE8 database. Figure 3a shows the fraction of the stable phases in the system at different temperatures. From the thermodynamic point of

view, it is possible to state that the only stable precipitate within the performed heat treatment temperature range in the alloy is of the type M_7C_3 , validating the results obtained by XRD. Moreover, EBSD was used for the characterization of individual secondary carbides (about 40 secondary carbides were randomly measured). In all cases an hexagonal crystallographic structure was detected, which corresponds to the M_7C_3 carbides (Figure 3b). The precipitation of $M_{23}C_6$ -type carbides might only be possible at temperatures under 738 K (465°C), whereas cementite (M_3C) is not expected to precipitate due to the high amount of Cr. Furthermore, it is well known that carbide-forming elements replace the less stable cementite, which dissolves into a finer alloy carbide dispersion [21]. This replacement by the alloy carbides, which is more resistant to coarsening, is able to produce an increase in hardness at higher temperatures [21]. The strengthening efficiency of this carbide dispersion will depend on the refinement of the precipitates and their volume fraction.

Figure 4 shows the microstructure for the as cast, SCD, Q and SCD+Q samples. The as cast microstructure is composed by primary austenite matrix surrounded by the eutectic mixture of M_7C_3 carbides/austenite, as also indicated in the diffractogram of Figure 2. Given the Cr and C content, no secondary carbides are expected to be observed in this sample. This microstructure is the starting point for the subsequent heat treatments previously described in Figure 1. SCD process produces a microstructure of ferrite and secondary carbides. The etching employed here (Villela's reagent) attacks the ferrite-carbide microstructure, therefore the optical image in Figure 4b shows dark regions corresponding to this type of microstructure, which is result of the high-concentration of small secondary carbides. The Q and SCD+Q microstructures (Figure 4c and Figure 4d) show a fine martensitic matrix surrounding the unchanged eutectic carbide phase when compared with as cast conditions. Small secondary carbides are expected to be present in

these samples, however, they cannot be resolved with optical microscopy techniques. Black and white arrows in Figure 4 indicate the regions of eutectic and secondary carbides, respectively. For better resolution and details of presence and distribution of secondary carbides, SEM images were acquired (Figure 5).

SEM images in BSE mode for all the samples taken at different scales are shown in Figure 5. As previously described, no secondary carbides are observed in the austenitic matrix of the as-cast condition. The destabilization treatment above the critical temperature 1253 K (980 °C) allow the precipitation of secondary carbides, as shown in SCD (Figure 5b), Q (Figure 5c) and SCD+Q (Figure 5d) samples. As learned from the XRD results, in the SCD sample, the secondary carbides are embedded in a ferritic matrix, whereas in the Q and SCD+Q samples in a martensitic matrix. In all cases the secondary carbides have apparently randomly nucleated and they show a round-like morphology.

The addition of a sub-critical diffusion (SCD) process following the destabilization step caused visible modifications compared to the as-cast material and also to quenched material. Large quantities of secondary carbides were precipitated within the austenitic matrix, which has transformed completely to ferrite by holding the temperature at 923 K (650 °C) (see Figure 2). Secondary carbides of different sizes can be observed embedded in the matrix. The prolonged duration of the SCD process allows the precipitation of a large quantity of new carbides and the growth of those precipitated during the destabilization step. This is clearly observable comparing Figure 5b and Figure 5c.

The Q and SCD+Q samples do not show a noticeable change in the amount of secondary carbides. However, the SCD+Q sample (Figure 5d) shows an apparent increase in size of secondary carbides inside the martensitic matrix (compared to the Q sample). The secondary carbides size was determined after image analysis (I-A) of SEM (BSE)

micrographs using the software A4i[®]. The calculated average carbide size was 0.44 μm and 0.51 μm for the Q and SCD+Q samples, respectively. The combination of a SCD state and quenching provides a coarse-sized secondary carbide distribution throughout the matrix, as indicated in the carbide size distribution of Figure 5 and also supported by the evidence observed by electron microscopy (Figure 4). This results from the sub-critical diffusion treatment which allows the secondary carbides to increase in size, mainly due to an extended time of energy input to the system.

Hardness and wear response evaluation

It is well known that the microstructure plays a fundamental role in the resulting mechanical properties. The wear resistance and mechanical properties, especially the hardness of HCCI depend on the type, morphology and distribution of carbides, and on the nature of the supporting matrix structure which, in turn, depends on the chemical composition and subsequent thermal treatments [14–16]. For this reason, the influence of the microstructure after thermal treatments in the wear response are being analyzed in this section.

The mechanical properties play a fundamental role in the applicability of these materials in the field. They would determine their machinability and subsequently, define the application in components. Specifically, microhardness measurements show the variations of local mechanical properties which may significantly influence the abrasion behavior of the material [30]. The macro and microhardness values of three different stages are represented in Figure 7a and Figure 7b, respectively. The expected change in macro-hardness due to the austenitic (as-cast sample) to martensitic (Q and SCD+Q samples) matrix change is clearly noticeable (Figure 7a). However, the presence of secondary carbides might not be dismissed as an influencing factor for this improvement. However, when comparing the results for the Q and SCD+Q samples, no significant changes are observed, since both present the same type of matrix. Thus, it is consequential to state that the main role regarding the mechanical properties is played by the matrix transformation. Micro-hardness measurements were performed on both, the matrix and the eutectic carbides. The same trend as in the macro-hardness measurements was observed when only the matrix is evaluated, as shown in Figure 7b. Additionally, a slight but not statistically representative increase in the matrix micro-hardness of the SCD+Q sample can be observed in comparison to the Q sample. However, when the eutectic

carbides zone is evaluated, both the carbides' intrinsic mechanical response and the surrounding matrix behavior are considered as a whole system due to the indentation size effects (Figure 7c). The same increase in micro-hardness is observable in the eutectic carbide areas of the SCD+Q respect to the Q sample. Those similar hardness values in Q and SCD+Q is mainly due to the precipitation of the same type of secondary carbides.

When comparing the micro-hardness of the eutectic carbide-containing regions of both heat treated samples to the as cast condition, the difference can be attributed to the increase in the supporting role of the matrix surrounding the eutectic carbides. It is worth noting that in all cases, an incoherent interface between the M_7C_3 phase and the matrix is expected, since the interatomic distances show a misfit larger than 25% [21]. This would further account for an efficient particle dispersion strengthening due to the effective hindering of dislocation mobility. Additionally, it has been reported that the quenching step adds a thermal strain to the matrix, which results in a dislocation punching during plastic strain and accounts for a significant strengthening [31].

Regarding the tribological behavior of the materials, the wear rates after pin on disc tests are shown in Figure 8. A significant reduction in wear rate of the Q and SCD+Q samples is observed when compared to the as-cast condition, being 45 and 83%, respectively. These results correlate quite well with the hypothesis that harder materials tend to show lower wear rates, given by the conventional Archard behavior/relationship [32]. However, both heat treated samples show a strongly differentiated wear behavior. Specifically, the SCD + Q sample showed a reduction of 69% compared to the quenched state.

This enhanced wear resistance of the SCD+Q sample cannot be explained by the macro- and micro-hardness values. It has already been reported that the wear behavior shows a

weak dependency on the macrostructure [26]. Thus, for the wear response of these type of materials (which should be considered as composite materials), not only the carbide structure or distribution should be considered, but also the nature of the matrix surrounding the carbides and their interaction as a whole must be taken into account. This synergistic effect is well-known in multimodal systems [19]. An important role in the improvement in wear response of Q and SCD+Q samples is played, as already shown for the hardness, by the austenite/martensite transformation of the matrix added to the secondary carbides precipitated on the treated samples. Furthermore, even in cases where a full martensitic transformation is not achieved, the amount of retained austenite might enhance the response by acting in two ways: inactivating the crack tip formation and hindering the crack development coming from more brittle phases [27].

During the wear test, oxidation occurs predominantly on the matrix parts of the track (Figure 9), whereas carbides are usually very slightly affected [33]. This oxidation leads to a continuous generation of hard and brittle wear particles that are consistently introduced to the sliding contact, thus inducing an oxide-driven transition from a mild to a severe third-body wear activity. Additionally, it has been reported for related systems that the wear rate decreases either with increasing carbide volume fraction (CVF) or with the increasing in carbide size for the same CVF [26]. In both heat treated samples, the total CVF is expected to be the same, since they present the same chemical composition. Yet, some difference was observed in the size distribution of the secondary carbides of both samples (as observed in Figure 6), being larger in the SCD+Q sample. Hence, these larger carbides provide an effective protection to the matrix (more wear-prone) from the abrasion. Additionally, it has been observed a higher crack density in carbides with the larger axis parallel to the wear surface [26], indicating a strong capacity of the carbides to absorb energy during friction. Then, it would be reasonable to expect that the sample

that shows a larger mean secondary carbide size will provide larger non-reactive areas of load support (in this case, the SCD+Q sample), would therefore present a lower wear rate.

Summarizing, this work shows that the application of a multi-step thermal treatment of a high chromium cast iron consisting of the austenite destabilization and a subsequent quenching, lead to the precipitation of carbides inducing a significant reduction in the wear loss by an accurate tailoring of the secondary phase. When compared to a traditional quenching process, the same matrix phase is obtained but with different mean secondary carbide size, which further translates into better wear response without sacrificing the overall mechanical properties.

Concluding remarks

In this study, we evaluated the effect of a destabilization treatment combined with a sub-critical diffusion and a quenching steps in the secondary carbides precipitation and their influence in the wear properties. It was observed, that HCCI in the as-cast condition composed by an austenitic matrix and eutectic carbides are not sufficient for a good abrasive wear resistance. In all cases, secondary carbides precipitated within the matrix are needed for an increase in wear response. A destabilization process followed by a SCD step allow not only the precipitation but also the growth of secondary carbides. An additional destabilization and quenching stages transform the matrix into martensite, resulting in a matrix with a higher hardness but no observable changes in secondary carbides. This process sequence also avoids the presence of ferrite (or pearlite) in the final microstructure, which would be detrimental for the mechanical properties. Finally, an improved wear resistance was observed in the SCD+Q sample compared to the Q one, being the size of secondary carbides apparently responsible for this behavior. For this, the

destabilization followed by a SCD is a fundamental step for the secondary carbides growth.

Wear mechanisms will be thoroughly analyzed in a further work, in order to evaluate the effect of microstructure changes in the wear rate and wear mechanisms, principally those related to the secondary carbides nature, shape and size.

Acknowledgements

This work was supported by the CREATE-Network Project, Horizon 2020 Program of the European Commission (RISE Project N° 644013).

The authors want to thank to Priv.-Doz. Dr. Jose Garcia from AB Sandvik Coromant R&D (Technology Area Manager Carbide and Sintering) for the helpful discussion and verification of some of the results.

References

- [1] R.J. Llewellyn, S.K. Yick, K.F. Dolman, Scouring erosion resistance of metallic materials used in slurry pump service, *Wear* 256 (2004) 592–599.
- [2] X.H. Tang, R. Chung, D.Y. Li, B. Hinckley, K. Dolman, Variations in microstructure of high chromium cast irons and resultant changes in resistance to wear, corrosion and corrosive wear, *Wear* 267 (2009) 116–121.
- [3] C. Scandian, C. Boher, J.D.B. de Mello, F. Rézai-Aria, Effect of molybdenum and chromium contents in sliding wear of high-chromium white cast iron: The relationship between microstructure and wear, *Wear* 267 (2009) 401–408.
- [4] ASTM International, A532 / A532M Standard Specification for Abrasion-Resistant Cast Irons, in: ASTM International, West Conshohocken, PA, 2003: pp. 1–4.
- [5] X. Zhi, J. Xing, Y. Gao, H. Fu, J. Peng, B. Xiao, Effect of heat treatment on microstructure and mechanical properties of a Ti-bearing hypereutectic high chromium white cast iron, *Mater. Sci. Eng. A* 487 (2008) 171–179.
- [6] ASM International, ed., *ASM Handbook, Volume 1: Properties and Selection: Irons, Steels, and High-Performance Alloys*, 10th ed., ASM International, 1990.
- [7] D. Li, L. Liu, Y. Zhang, C. Ye, X. Ren, Y. Yang, et al., Phase diagram calculation of high chromium cast irons and influence of its chemical composition, *Mater. Des.* 30 (2009) 340–345.
- [8] A. Bedolla-Jacuinde, R. Correa, I. Mejía, J.G. Quezada, W.M. Rainforth, The effect of titanium on the wear behaviour of a 16%Cr white cast iron under pure sliding, *Wear*. 263 (2007) 808–820.
- [9] R.J. Chung, X. Tang, D.Y. Li, B. Hinckley, K. Dolman, Effects of titanium addition on microstructure and wear resistance of hypereutectic high chromium cast iron Fe–25wt.%Cr–4wt.%C, *Wear*. 267 (2009) 356–361.
- [10] J. Wang, R.L. Zuo, Z.P. Sun, C. Li, H.H. Liu, H.S. Yang, et al., Influence of secondary carbides precipitation and transformation on hardening behavior of a 15 Cr-1 Mo-1.5 v white iron, *Mater. Charact.* 55 (2005) 234–240.
- [11] M. Filipovic, Z. Kamberovic, M. Korac, M. Gavrilovski, Microstructure and

- mechanical properties of Fe–Cr–C–Nb white cast irons, *Mater. Des.* 47 (2013) 41–48.
- [12] S.H. Mousavi Anijdan, A. Bahrami, N. Varahram, P. Davami, Effects of tungsten on erosion–corrosion behavior of high chromium white cast iron, *Mater. Sci. Eng. A.* 454–455 (2007) 623–628.
- [13] J. Wang, J. Xiong, H. Fan, H.-S. Yang, H.-H. Liu, B.-L. Shen, Effects of high temperature and cryogenic treatment on the microstructure and abrasion resistance of a high chromium cast iron, *J. Mater. Process. Technol.* 209 (2009) 3236–3240.
- [14] D. Kopyci, E. Guzik, D. Siekaniec, A. Szcz, Analysis of the High Chromium Cast Iron Microstructure after the Heat Treatment, 14 (2014) 43–46.
- [15] A. Wiengmoon, J.T.H. Pearce, T. Chairuangstri, Relationship between microstructure , hardness and corrosion resistance in 20 wt .% Cr , 27 wt .% Cr and 36 wt .% Cr high chromium cast irons, *Mater. Chem. Phys.* 125 (2011) 739–748.
- [16] S.D. Carpenter, D. Carpenter, J.T.H. Pearce, XRD and electron microscope study of an as-cast 26.6 % chromium white iron microstructure, 85 (2004) 32–40.
- [17] M. Duarte, J. Molina, R. Prieto, E. Louis, J. Narciso, Effects of particle size and volume fraction on wear behavior of aluminum alloys/ceramic particles composites, in: *Solidif. Process. Met. Matrix Compos.*, 2006 TMS Annual Meeting, San Antonio, TX; United States, 2006: pp. 249–257.
- [18] C. García-Cordovilla, J. Narciso, E. Louis, Abrasive wear resistance of aluminium alloy/ceramic particulate composites, *Wear.* 192 (1996) 170–177.
- [19] A. Demir, N. Altinkok, F. Findik, I. Ozsert, The Wear Behaviour of Dual Ceramic Particles ($\text{Al}_2\text{O}_3/\text{SiC}$) Reinforced Aluminium Matrix Composites, *Key Eng. Mater.* 264–268 (2004) 1079–1082.
- [20] S. Kumar, R.S. Panwar, O.P. Pandey, Effect of dual reinforced ceramic particles on high temperature tribological properties of aluminum composites, *Ceram. Int.* 39 (2013) 6333–6342.
- [21] D.A. Porter, K.E. Easterling, *Phase Transformations in Metals and Alloys*, CRC Press, 1992.
- [22] Z. Sun, R. Zuo, C. Li, B. Shen, J. Yan, S. Huang, TEM study on precipitation and

- transformation of secondary carbides in 16Cr-1Mo-1Cu white iron subjected to subcritical treatment, *Mater. Charact.* 53 (2004) 403–409.
- [23] M. Filipovic, Z. Kamberovic, M. Korac, M. Gavrilovski, Correlation of microstructure with the wear resistance and fracture toughness of white cast iron alloys, *Met. Mater. Int.* 19 (2013) 473–481.
- [24] A. Wiengmoon, T. Chairuangsi, A. Brown, R. Brydson, D.V. Edmonds, J.T.H. Pearce, Microstructural and crystallographical study of carbides in 30wt.%Cr cast irons, *Acta Mater.* 53 (2005) 4143–4154.
- [25] A.E. Karantzalis, A. Lekatou, H. Mavros, Microstructural Modifications of As-Cast High-Chromium White Iron by Heat Treatment, *J. Mater. Eng. Perform.* 18 (2009) 174–181.
- [26] Ö.N. Doğan, J. a. Hawk, G. Laird, Solidification structure and abrasion resistance of high chromium white irons, *Metall. Mater. Trans. A.* 28 (1997) 1315–1328.
- [27] H. Gasan, F. Erturk, Effects of a Destabilization Heat Treatment on the Microstructure and Abrasive Wear Behavior of High-Chromium White Cast Iron Investigated Using Different Characterization Techniques, *Metall. Mater. Trans. A.* 44 (2013) 4993–5005.
- [28] J.Q. Xu, Y.Y. Chen, W. Wang, K.P. Liu, H.S. Liu, Y.D. Xiao, Sliding friction properties of austenite-and martensite-based white cast iron containing 8.5% chromium, *J. Mater. Sci.* 45 (2010) 6108–6114.
- [29] J.D.B. DeMello, M. Durand-Charre, S. Hamar-Thibault, Solidification and solid state transformations during cooling of chromium-molybdenum white cast irons, *Metall. Trans. A.* 14 (1983) 1793–1801.
- [30] J. Chen, M. Lv, S. Tang, Z. Liu, G. Wang, Correlation between mechanical properties and retained austenite characteristics in a low-carbon medium manganese alloyed steel plate, *Mater. Charact.* 106 (2015) 108–111.
- [31] K.K. Chawla, *Composite Materials: Science and Engineering*, 3rd ed., Springer New York, 2012.
- [32] H. Czichos, K.-H. Habig, *Tribologie Handbook*, 2nd., Friedr. Vieweg & Son Verlag, 2003.
- [33] S. Atapek, S. Polat, A study of wear of high-chromium cast iron under dry friction,

Met. Sci. Heat Treat. 55 (2013) 181–183.

List of Figures

Figure 1: schematic representation for the different thermal treatments (a) quenching, (b) sub-critical diffusion and (c) sub-critical diffusion followed by quenching.

Figure 2: XRD diffractograms for the different thermal treatments. The inset in the image shows the shift and peak width of the martensite diffraction peaks (samples Q and SCD+Q) respect to that from the ferrite (sample SCD).

Figure 3: a) Phase fraction vs temperature diagram, calculated with Thermocalc and b) Kikuchi patterns corresponding to the secondary carbides showing the hexagonal crystallographic structure (M_7C_3 type).

Figure 4: Optical microscopy images showing: (a) the as cast condition; (b) the SCD sample (c) the Q sample; (d) the SCD+Q sample. The samples were etched with Vilella reagent for matrix/carbide contrast. Black arrows indicate the regions of eutectic carbides and the white arrows indicate regions of secondary carbides.

Figure 5: SEM (BSE) Images for all the samples at different magnifications from left to right 500X, 2000X and 6500X, respectively. a) as cast, b) SCD, c) Q and d) SCD+Q.

Figure 6: secondary carbides size distribution obtained after image analysis of SEM (BSE) images.

Figure 7: (a) Hardness test results in the Rockwell C Scale and (b) micro-hardness measurements for three microstructural states: as Cast, Q and SCD + Q. Standard deviation of the measures is also plotted. (c) Optical micrograph showing the area influenced by the micro indentation during the eutectic zone measurement.

Figure 8: wear rate volume in $mm^2 \cdot N^{-1}$ calculated after pin on disc test for the different treated samples.

Figure 9: (a) Backscattered electron micrograph of the wear track in the As-Cast sample
(b) wear track of the quenched sample. The darker areas are tribologically induced oxides, whereas the lighter regions are either carbides or unmodified matrix material. The white arrows indicate regions where the eutectic carbides remain unworn.

Figure 1

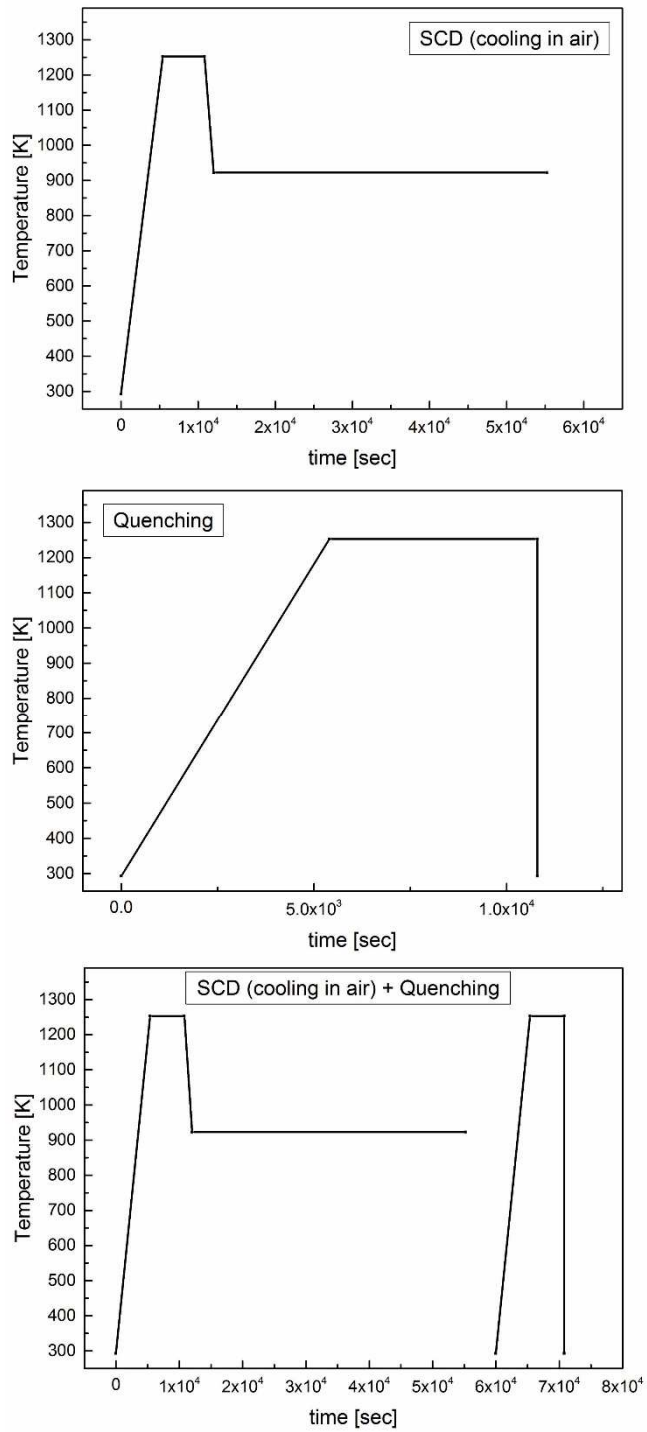


Figure 2

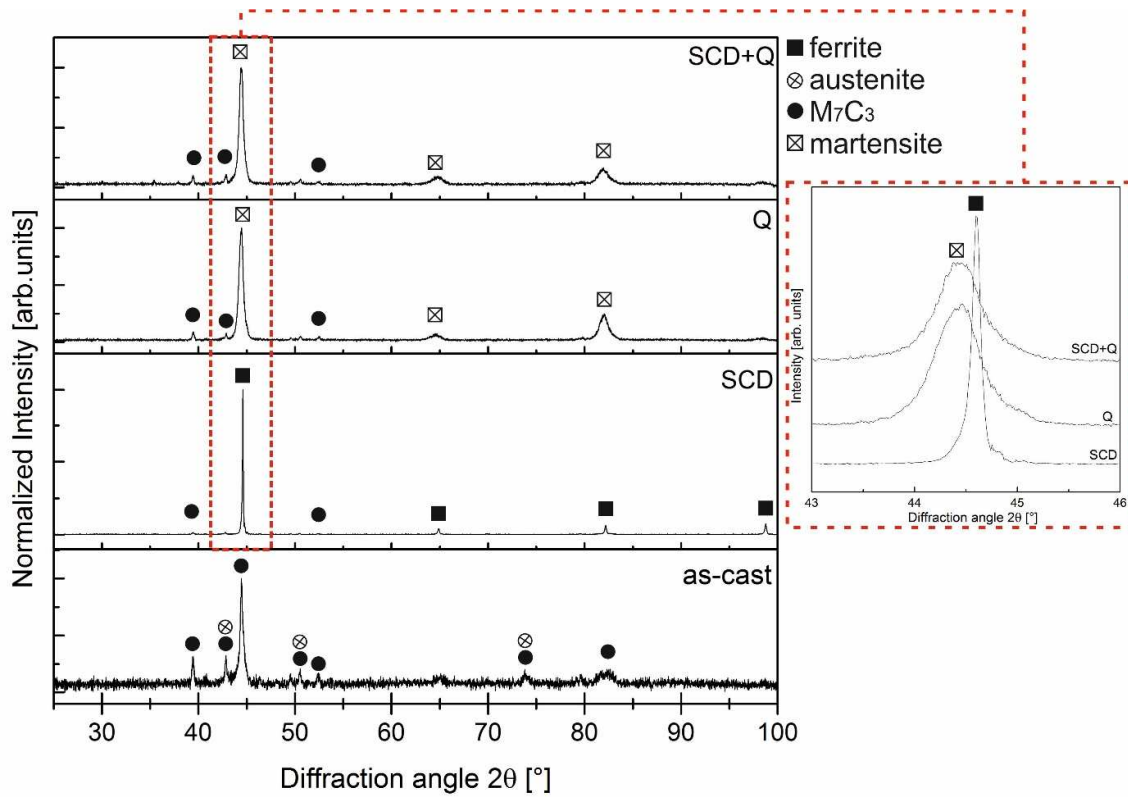


Figure 3

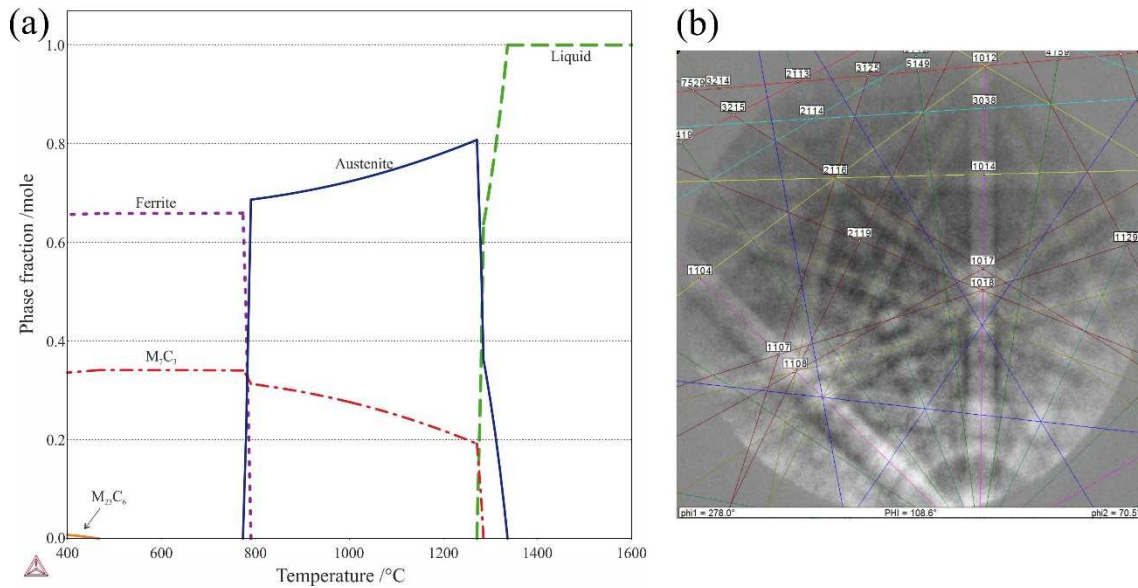


Figure 4

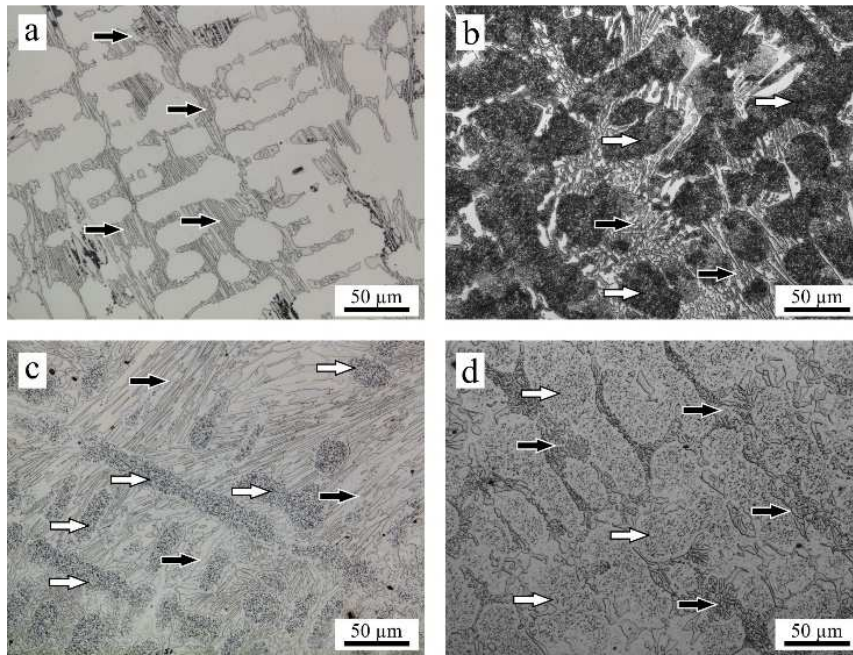


Figure 5

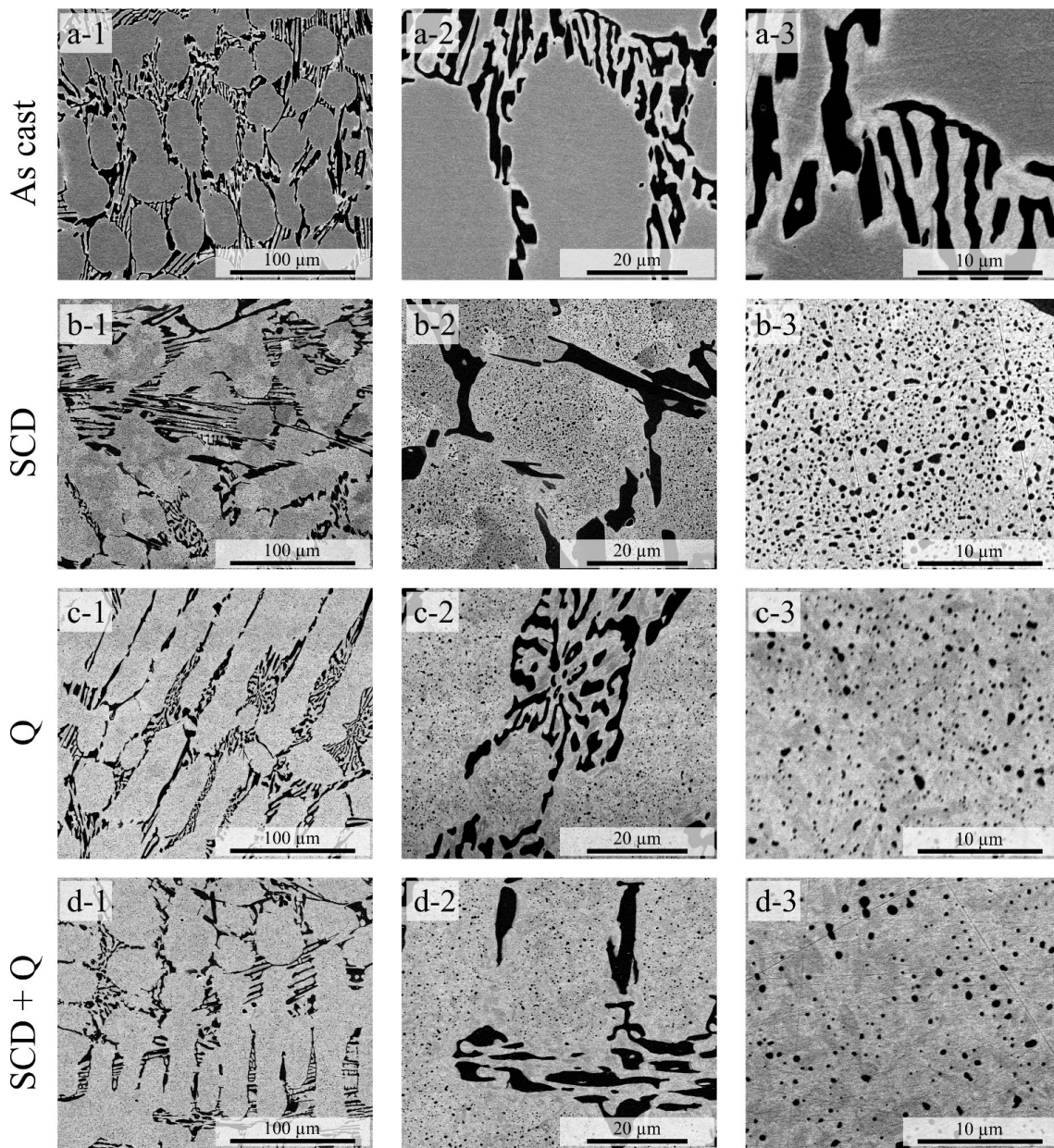


Figure 6

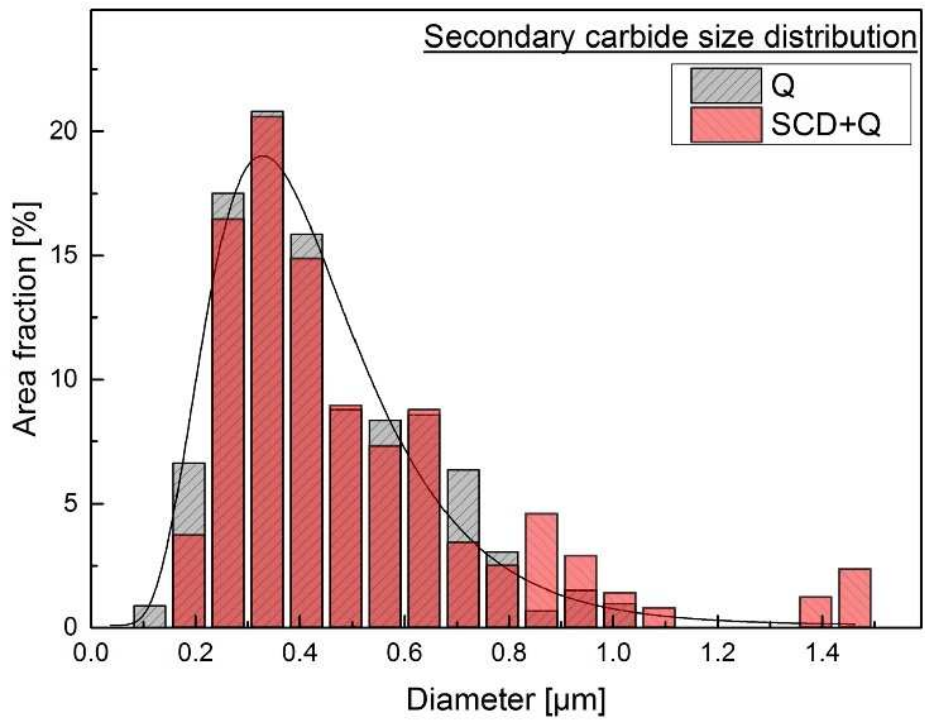


Figure 7

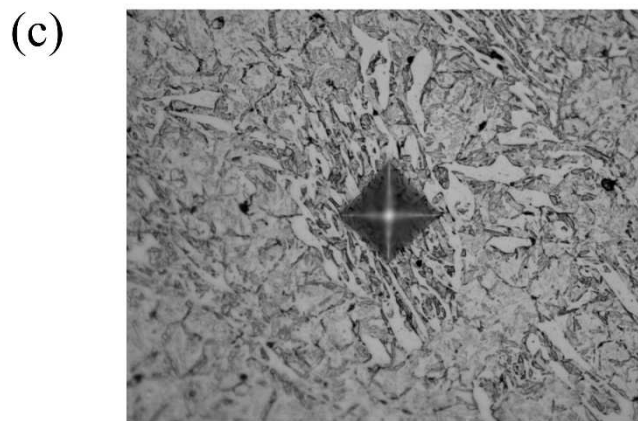
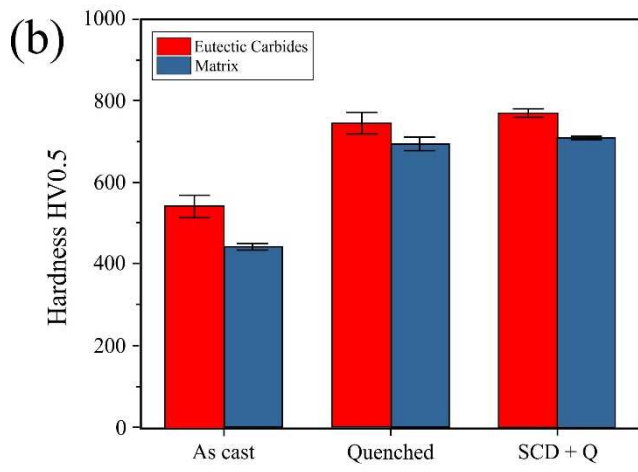
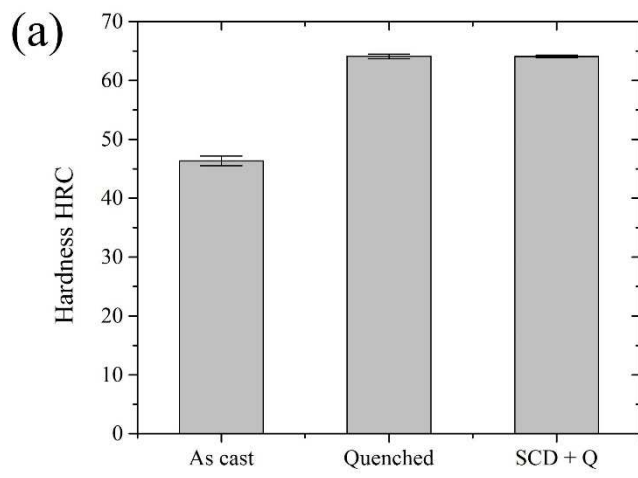


Figure 8

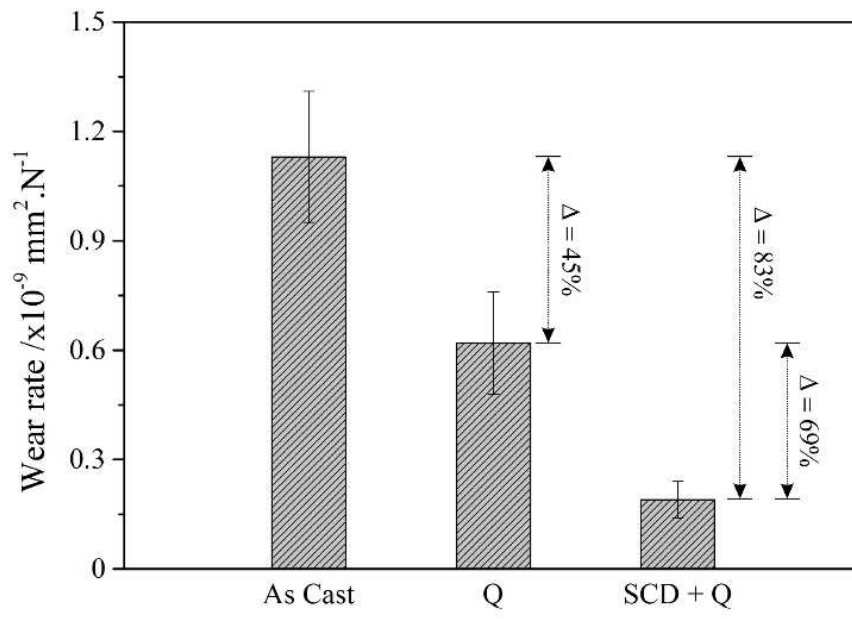


Figure 9

